SUPPLEMENTARY DATA

Targeted *in vivo* Imaging of Integrin $\alpha_v\beta_6$ with an Improved Radiotracer and its Relevance in a Pancreatic Tumor Model

Sven H. Hausner, Craig K. Abbey, Richard J. Bold, M. Karen Gagnon, Jan Marik, John F. Marshall, Cathy E. Stanecki, and Julie L. Sutcliffe

Peptide synthesis and radiolabeling. Synthesis of A20FMDV2 (NAVPNLRGDLQVLAQKVART) and peptide purification followed previously described methods (1). In an effort to reduce the amount of Fmoc-PEG_{28}-COOH (FW = 1544.8; NovaBiochem) required, this compound was coupled in an overall ratio of 1.65:1 for Fmoc-PEG_{28}-COOH/peptide on resin, split into two 18 h-coupling cycles (1.1:1 and 0.55:1 ratios, respectively). *N*,*N*,*N*',*N*'-Tetramethyl-*O*-(7-azabenzotriazol-1-yl)uranium hexafluorophosphate (HATU, GL Biochem) and DIPEA were used as coupling reagents.

N-terminal labeling with 4-[^{19}F]fluorobenzoic acid followed standard HBTU/DIPEA procedures. Non-radiolabeled compounds were characterized by matrix-assisted laser desorption/ionization (MALDI) mass spectrometry (Supplementary Fig. S1, S2).

Peptides were N-terminally radiolabeled on solid phase as previously described (1, 2). Radiotracer purity and identity were assessed by HPLC (Supplementary Fig S1, S2).

Supplementary Table S1. Biodistribution data for the radiotracers after i.v. injection into male *nu/nu* mice in the BxPC-3 model and the DX3puro/DX3puroβ6 model (n = 3/time point/radiotracer /model). Data are expressed as % ID/g ± SD.

Tissue	[^{18}F]FBA-A20FMDV2			[^{18}F]FBA-PEG$_{28}$-A20FMDV2			[^{18}F]FBA-(PEG$_{28}$)$_2$-A20FMDV2		
	1 h	2 h	4 h	1 h	2 h	4 h	1 h	2 h	4 h
Gall bladder	10.89 ± 2.06	9.73 ± 2.52	4.55 ± 3.91	3.87 ± 1.69	0.91 ± 0.88	0.56 ± 0.92	0.90 ± 0.52	1.07 ± 0.57	1.47 ± 0.34
Muscle	0.54 ± 0.18	0.30 ± 0.19	0.05 ± 0.02	0.75 ± 0.47	0.58 ± 0.14	0.41 ± 0.09	0.38 ± 0.03	0.69 ± 0.03	0.47 ± 0.06
Bone	0.40 ± 0.22	0.15 ± 0.07	0.09 ± 0.05	0.66 ± 0.44	0.20 ± 0.28	0.20 ± 0.06	0.10 ± 0.05	0.41 ± 0.12	0.30 ± 0.09
Kidneys	3.29 ± 0.81	1.03 ± 0.76	0.16 ± 0.09	18.97 ± 5.06	7.44 ± 1.76	3.28 ± 0.72	42.57 ± 12.97	41.14 ± 6.72	41.53 ± 4.60
Liver	0.27 ± 0.07	0.08 ± 0.02	0.02 ± 0.00	0.16 ± 0.05	0.12 ± 0.03	0.05 ± 0.02	0.19 ± 0.02	0.18 ± 0.04	0.18 ± 0.01
Blood	0.21 ± 0.07	0.07 ± 0.01	0.02 ± 0.01	0.16 ± 0.02	0.05 ± 0.02	0.03 ± 0.03	0.18 ± 0.10	0.09 ± 0.02	0.01 ± 0.01
Pancreas	0.16 ± 0.01	0.04 ± 0.02	0.01 ± 0.01	0.45 ± 0.25	0.15 ± 0.08	0.06 ± 0.02	0.28 ± 0.16	0.44 ± 0.20	0.47 ± 0.26
BxPC3 ($\alpha_v\beta_6$ +)	0.69 ± 0.19	0.32 ± 0.03	0.12 ± 0.03	1.85 ± 0.44	1.33 ± 0.14	1.48 ± 0.04	1.57 ± 0.25	2.28 ± 0.54	2.08 ± 0.37
Ratio BxPC3/ Muscle	1.3:1[§]	1.1:1[§]	2.5:1[€]	2.5:1[€]	2.3:1[†]	3.6:1[¶]	4.1:1[†]	3.3:1[†]	4.4:1[†]
Ratio BxPC3/ Blood	3.3:1[€]	4.7:1[‡]	7.0:1[†]	11.8:1[†]	24.8:1[¶]	47.9:1[¶]	9.0:1[‡]	26.6:1[†]	150:1[‡]
Ratio BxPC3/ Pancreas	4.4:1[†]	9.0:1[‡]	9.5:1[†]	4.2:1[†]	8.8:1[‡]	23.6:1[¶]	5.6:1[†]	5.2:1[†]	4.4:1[†]
DX3puroβ6 ($\alpha_v\beta_6$ +)	0.66 ± 0.09[*]	0.28 ± 0.03[*]	0.06 ± 0.00[*]	0.49 ± 0.12	0.42 ± 0.05	0.49 ± 0.04	0.52 ± 0.09	0.61 ± 0.11	0.54 ± 0.08[#]
DX3puro ($\alpha_v\beta_6$ -)	0.21 ± 0.07[*]	0.07 ± 0.02[*]	0.02 ± 0.01[*]	0.10 ± 0.03	0.05 ± 0.00	0.07 ± 0.06	0.11 ± 0.03	0.09 ± 0.03	0.06 ± 0.01[#]
Ratio DX3puroβ6/ DX3puro	3.1:1[†]	4.3:1[‡]	3.8:1[‡]	4.6:1[†]	8.0:1[‡]	6.6:1[‡]	4.9:1[†]	6.9:1[†]	9.2:1[¶]

[§] $P > 0.05$ (not significant)

[€] $P < 0.05$

[†] $P < 0.01$

[‡] $P < 0.001$

[¶] $P < 0.0001$

[*] Data from (1).

[#] $n = 5$

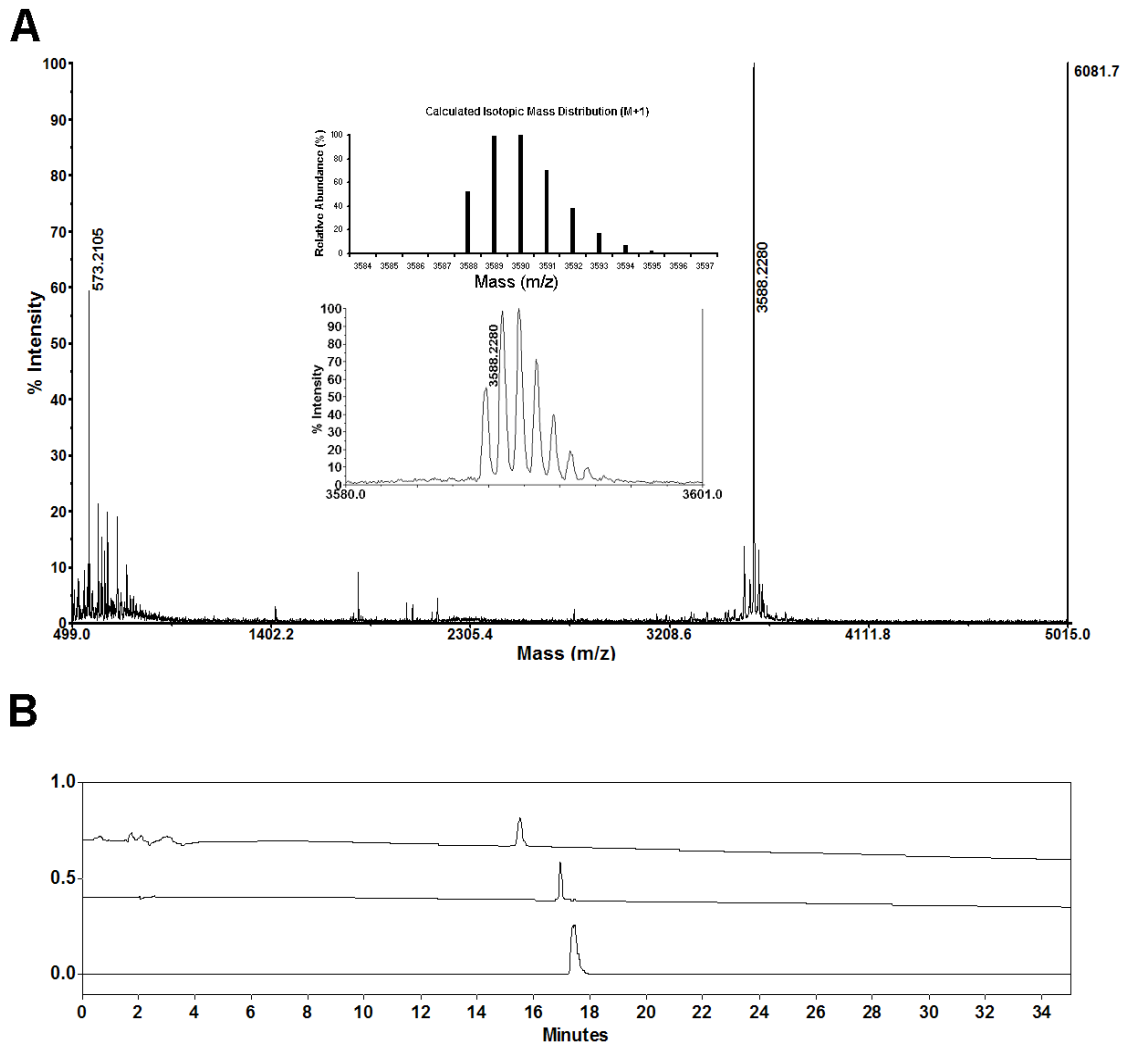

Supplementary Figure S1. Analytical data for FBA-PEG_{28}-A20FMDV2. *A*, MALDI-Mass spectrum of [^{19}F]FBA-PEG_{28}-A20FMDV2 (FW_{exp} : 3588.2280; $FW_{calc(M+1)}$: 3588.0401) demonstrating the monodisperse nature of the incorporated PEG. A close up view reveals the isotopic distribution (bottom insert), closely matching the calculated distribution for $C_{159}H_{285}FN_{33}O_{57}$ (top insert). Low molecular weight signals were caused by the MALDI matrix. *B*, HPLC traces of the radiotracer ([^{18}F]FBA-PEG_{28}-A20FMDV2, $R_{t(PMT)}$ = 17.4 min; bottom), the nonradioactive standard ([^{19}F]FBA-PEG_{28}-A20FMDV2, $R_{t(220nm)}$ = 17.0 min; middle), and the non-FBA-bearing precursor (H_2N-PEG_{28}-

A20FMDV2, $R_{t(220nm)}$ = 15.5 min; top). Note the increase of about 1.5 minutes in retention time caused by introduction of the FBA moiety. The slight difference in retention times between the nonradioactive standard and the radiotracer was caused by the serial setup of the UV- and the radiation-detector. The radio-HPLC is representative for 7 independent syntheses (radiochemical purity: >97%, decay-corrected radiochemical yield: 6.4 ± 2.0%, specific activity: >1Ci/μmol). HPLC parameters: 9% solvent B isocratic for 2 min, then linear increase to 81% over 30 min at a flow rate of 1.5 mL/min using a Jupiter Proteo (Phenomenex) reverse phase column (90Å, 250 mm × 4.6 mm × 4 μm). Solvent A: 0.05% TFA in water (v/v); solvent B: acetonitrile. X-axis: Retention times (min). Y-axis: arbitrary units.

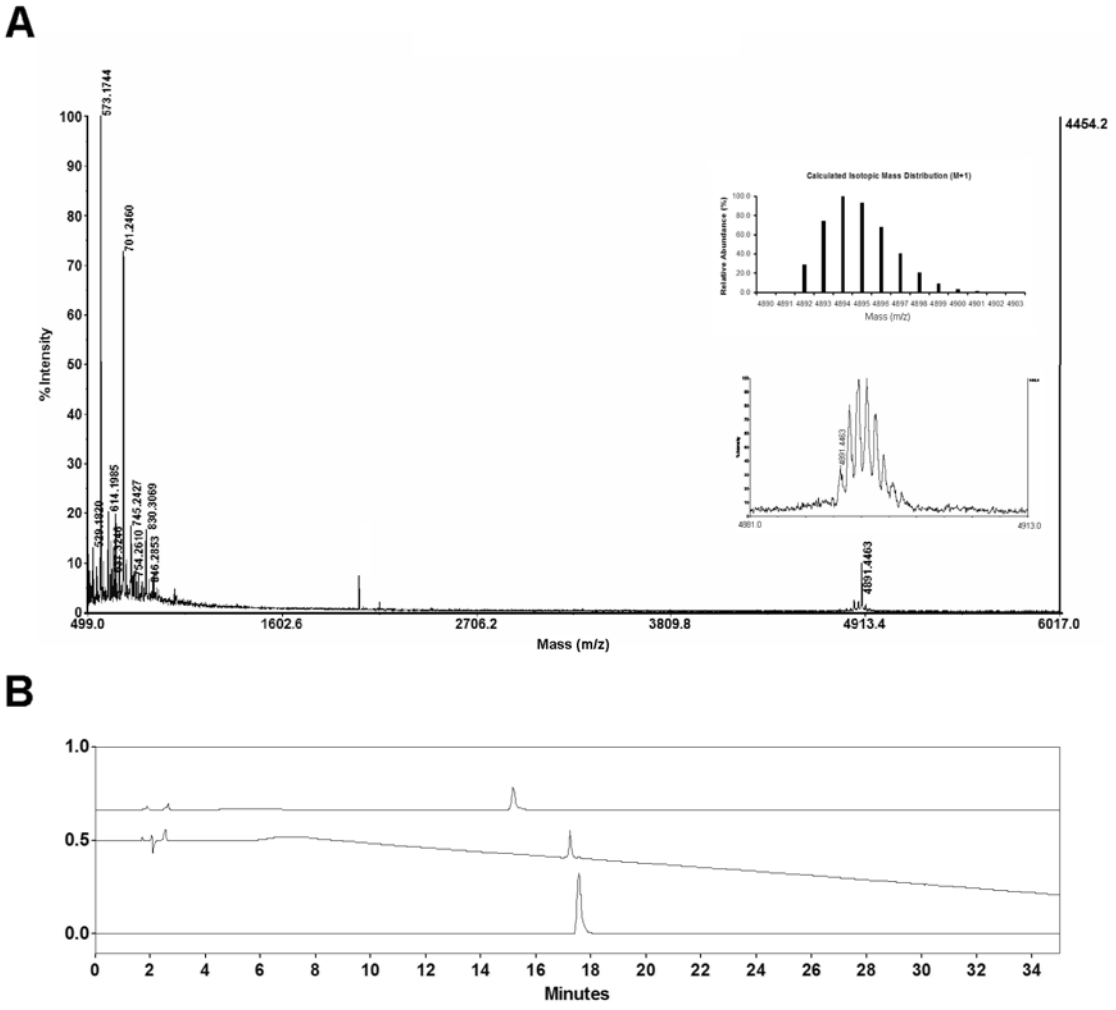

Supplementary Figure S2. Analytical data for FBA-$(PEG_{28})_2$-A20FMDV2. *A*, MALDI-Mass spectrum of [^{19}F]FBA-$(PEG_{28})_2$-A20FMDV2 (FW_{exp} : 4891.4463; $FW_{calc(M+1)}$: 4891.8114) demonstrating the monodisperse nature of the incorporated PEG. A close up view reveals the isotopic distribution (bottom insert), closely matching the calculated distribution for $C_{218}H_{402}FN_{34}O_{86}$ (top insert). Low molecular weight signals were caused by the MALDI matrix. *B*, HPLC traces of the radiotracer ([^{18}F]FBA-$(PEG_{28})_2$-A20FMDV2, $R_{t(PMT)}$ = 17.6 min; bottom), the nonradioactive standard

([^{19}F]FBA-$(PEG_{28})_2$-A20FMDV2, $R_{t(220nm)}$ = 17.3 min; middle), and the non-FBA-bearing precursor (H_2N-$(PEG_{28})_2$-A20FMDV2, $R_{t(220nm)}$ = 15.2 min; top). Note the increase of about two minutes in retention time caused by introduction of the FBA moiety. The slight difference in retention times between the nonradioactive standard and the radiotracer was caused by the serial setup of the UV- and the radiation-detector. The radio-HPLC is representative for 12 independent syntheses (radiochemical purity: >97%, decay-corrected radiochemical yield: 5.4 ± 2.5%, specific activity: >1Ci/μmol). HPLC parameters: Same as for Supplementary Figure S1. X-axis: Retention times (min). Y-axis: arbitrary units.

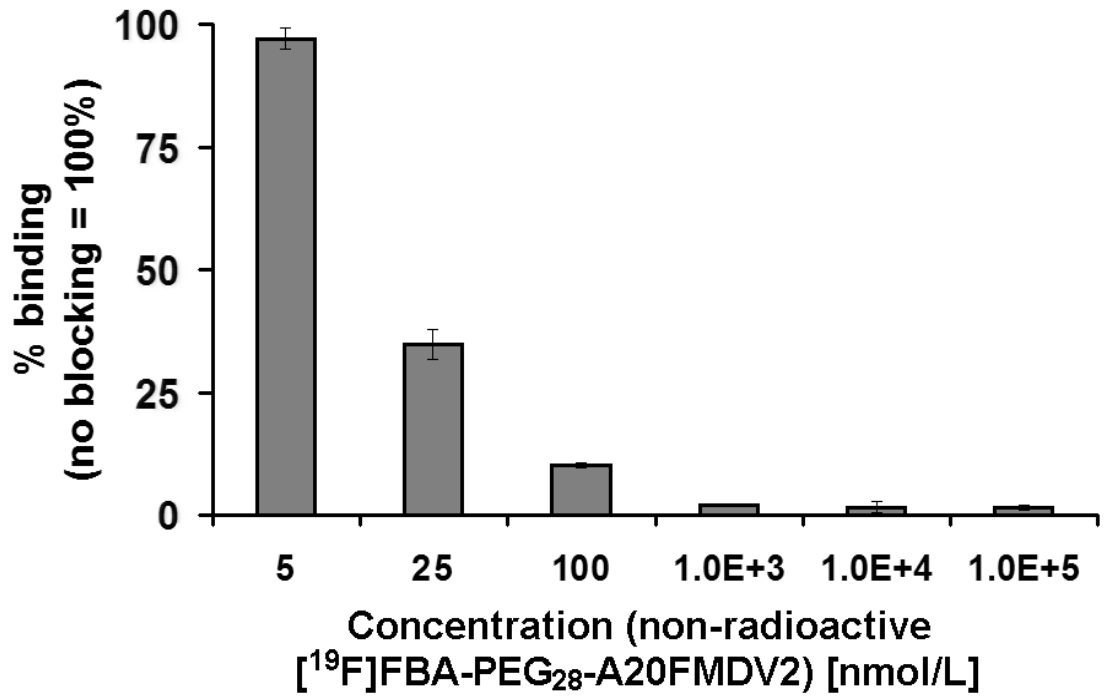

Supplementary Figure S3. Blocking of binding of the radiotracer [^{18}F]FBA-PEG$_{28}$-A20FMDV2 to the $\alpha_v\beta_6$-expressing DX3puroβ6 cell line using non-radioactive [^{19}F]FBA-PEG$_{28}$-A20FMDV2. Cells were incubated for one hour in the presence of the radiotracer together with non-radioactive [^{19}F]FBA-PEG$_{28}$-A20FMDV2 at the concentrations indicated; an assay without non-radioactive [^{19}F]FBA-PEG$_{28}$-A20FMDV2 was run concurrently for comparison (n = 3 samples/cell line/condition). Following removal of the supernatant and washing of the cell pellet, the amount of bound radioactivity was determined using a γ-counter. The plot represents triplicate experiments with 3.75 × 10^6 cells at each condition. Binding of [^{18}F]FBA-PEG$_{28}$-A20FMDV2 to DX3puroβ6 cells was blocked completely by non-radioactive [^{19}F]FBA-PEG$_{28}$-A20FMDV2 at concentrations ≥1 μmol/L. *Filled bars*, % radioactivity bound to cells relative to un-blocked conditions; *thin bars*, SD.

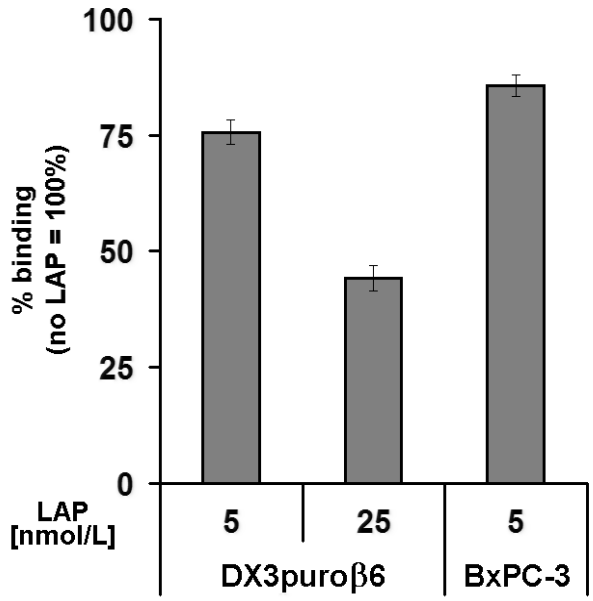

Supplementary Figure S4. Evaluation of the effect of LAP on binding of the radiotracer [^{18}F]FBA-PEG$_{28}$-A20FMDV2 to the $\alpha_v\beta_6$-expressing DX3puroβ6 and BxPC-3 cell lines. Cells were incubated for one hour in the presence of the radiotracer together with LAP at the concentrations indicated; assays without LAP were run concurrently for comparison (n = 3 samples/cell line/condition). Following removal of the supernatant and washing of the cell pellet, the amount of bound radioactivity was determined using a γ-counter. The plot represents triplicate experiments with 3.75 × 10^6 cells at each condition. The data demonstrate efficient binding of [^{18}F]FBA-PEG$_{28}$-A20FMDV2 even in the presence of LAP. *Filled bars*, % radioactivity bound to cells relative to LAP-free conditions; *thin bars*, SD.

Supplementary Data References.

1 Hausner SH, DiCara D, Marik J, Marshall JF, Sutcliffe JL. Use of a peptide derived from foot-and-mouth disease virus for the noninvasive imaging of human cancer: Generation and evaluation of 4-[^{18}F]fluorobenzoyl A20FMDV2 for *in vivo* imaging of integrin $\alpha_v\beta_6$ expression with positron emission tomography. Cancer Res 2007;67:7833-40.

2 Sutcliffe-Goulden JL, O'Doherty MJ, Marsden PK, Hart IR, Marshall JF, Bansal SS. Rapid solid phase synthesis and biodistribution of ^{18}F-labelled linear peptides. Eur J Nucl Med Mol Imaging 2002;29:754-9.